Statistical projection effects in a hydrodynamic pilot-wave system

Pedro J. Sáenz, Tudor Cristea-Platon and John W. M. Bush*

Millimetric liquid droplets can walk across the surface of a vibrating fluid bath, self-propelled through a resonant interaction with their own guiding or 'pilot' wave fields. These walking droplets, or 'walkers', exhibit several features previously thought to be peculiar to the microscopic, quantum realm. In particular, walkers confined to circular corrals manifest a wave-like statistical behaviour reminiscent of that of electrons in quantum corrals. Here we demonstrate that localized topological inhomogeneities in an elliptical corral may lead to resonant projection effects in the walker's statistics similar to those reported in quantum corrals. Specifically, we show that a submerged circular well may drive the walker to excite specific eigenmodes in the bath that result in drastic changes in the particle's statistical behaviour. The well tends to attract the walker, leading to a local peak in the walker's position histogram. By placing the well at one of the foci, a mode with maxima near the foci is preferentially excited, leading to a projection effect in the walker's position histogram towards the empty focus, an effect strongly reminiscent of the quantum mirage. Finally, we demonstrate that the mean pilot-wave field has the same form as the histogram describing the walker's statistics.

Since the groundbreaking experiments of Yves Couder, Emmanuel Fort and co-workers[1,2], significant effort has been devoted to examining the potential and limitations[3] of walking droplets as a hydrodynamic quantum analogue system[4]. Harris et al. demonstrated that the chaotic motion of a walker confined to a circular cavity, or 'corral', may lead to the emergence of a wave-like statistical behaviour, with the droplet's position histogram being prescribed by the eigenmode of the cavity[5], reminiscent of the probability distribution of a two-dimensional electron gas confined to a circular quantum corral[6]. Despite several attempts[7–9], a conclusive theoretical demonstration of this robust statistical behaviour remains an open challenge. The results in the circular corral[5] suggest the possibility of establishing deeper connections between these two markedly different systems.

The Kondo effect[10,11] is the suppression in the local differential conductance of a metallic substrate due to the presence of magnetic impurities. In a remarkable recent set of experiments, Manoharan and co-workers[12] exploited this effect to demonstrate that, due to the special resonant properties of elliptical corrals, an individual atom (magnetic impurity) inside a quantum corral can be used to control the relative importance of specific cavity modes, thus allowing for the production of arbitrary superpositions of spatial quantum states[12]. When the magnetic impurity is placed at one focus, a particular elliptical eigenmode with extrema near the foci is preferentially excited, leading to a heightened statistical response in the electron density near the empty focus. Owing to the acute sensitivity of the differential conductance to the statistical response, the result is the projection of a pronounced minimum in the differential conductance from the occupied focus to the empty one, the so-called quantum mirage[13]. Here, we demonstrate that similar mode superposition and projection effects can be induced and manipulated in the walking droplet system by using a submerged circular well in the role of the magnetic impurity.

A schematic of the experimental set-up is shown in Fig. 1. An elliptical corral made of stainless steel was filled with 20 cSt silicon oil with density $\rho = 950\,\mathrm{kg\,m^{-3}}$, viscosity $\nu = 20.9\,\mathrm{cSt}$ and surface tension $\sigma = 20.6\,\mathrm{mN\,m^{-1}}$. The eccentricity of the ellipse is $e = 0.5$ and the length of its semi-major axis is $a = 14.25\,\mathrm{mm}$. The corral

was filled to a height $h = 1.70 \pm 0.05\,\mathrm{mm}$ such that a very thin liquid film of depth $h_1 = 0.05 \pm 0.03\,\mathrm{mm}$ overlays the border of the cavity, serving as a wave damper. The bath was mounted on an optical table and vibrated vertically by an electromagnetic shaker with acceleration $\Gamma(t) = \gamma \cos(\omega t)$, where γ and $f = \omega/2\pi$ are the prescribed maximum acceleration and frequency, respectively. Unless otherwise noted, the driving frequency was fixed at $f = 72\,\mathrm{Hz}$. The shaker was connected to the bath by a thin steel rod coupled with a linear air bearing to ensure a spatially uniform vibration to within 0.1% (ref. [14]). The forcing was monitored by two accelerometers, attached to the bath on opposite sides of the drive shaft, and a closed-loop feedback ensured a constant acceleration amplitude to within $\pm 0.002g$ (ref. [14]). A droplet of the same silicon oil with diameter $d = 0.79 \pm 0.01\,\mathrm{mm}$ was generated with a piezoelectric droplet-on-demand generator and placed on the vibrating bath with the help of a removable slide[15]. Provided the driving acceleration was in the appropriate range, the drop could survive indefinitely by bouncing on the surface of the bath[16]. To ensure that ambient air currents did not affect the results, the corral was sealed with a transparent acrylic lid. We note that, although previous studies of walking droplets have considered the deep-water regime ($h > 4\,\mathrm{mm}$ for the vibrational frequencies typically examined), we considered a relatively shallow layer in order to exploit variable bottom topography as a means of altering the drop's statistical behaviour.

The walker motion was recorded at 20 frames per second with a charge-coupled device (CCD) camera mounted directly above the bath and tracked with an in-house particle-tracking algorithm. The bath was illuminated with a light-emitting diode (LED) light ring to increase the contrast between the drop and the black background. This visualization set-up is optimal for droplet tracking but does not allow for observation of the wave field. The simplest method to capture the wave form is to view the normal reflection of light at the free surface[17]. To that end, a semi-reflective mirror at 45° was placed between the CCD camera and the bath, and the light ring was replaced by a diffuse-light lamp facing the mirror horizontally. Images can then be observed with bright regions corresponding to horizontal parts of the surface, extrema or saddle points[17] (Fig. 2a,b). The wave field was recorded at frequency $f/4$.

Department of Mathematics, Massachusetts Institute of Technology, Cambridge, MA 02139, USA. *e-mail: bush@math.mit.edu
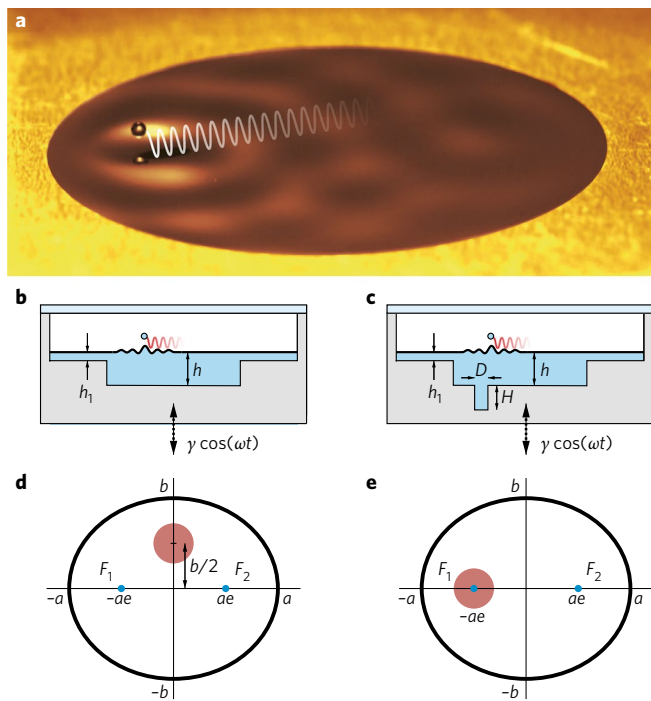
Fig. 1 | Schematic of the experimental set-up. a, Oblique view of a droplet and its pilot wave exploring an elliptical corral. **b,c,** Cross-section of the topologically homogeneous elliptical corral (**b**) and the elliptical corral with a submerged circular well of depth $H = 4.5$ mm and diameter $D = 5.5$ mm (**c**). The liquid depth in the corral and in the wave damper is $h = 1.70$ mm and $h_1 = 0.05$ mm, respectively. **d,e,** Location of the circular well corresponding to the results presented in the left and right columns of Fig. 5. The length of the semi-major axis and eccentricity of the ellipse are $a = 14.25$ mm and $e = \sqrt{1 - b^2/a^2} = 0.5$, respectively.

When the driving acceleration exceeds the Faraday threshold γ_F, which depends on f, h, the fluid properties and cavity size, the bath spontaneously becomes unstable to a standing field of subharmonic Faraday waves[18,19]. A critical parameter of the system is the so-called 'memory', γ/γ_F, which indicates the proximity of the driving acceleration to the Faraday threshold and so prescribes the longevity of the waves excited by the drop at each impact[20]. In the high-memory regime ($\gamma \to \gamma_F^-$), the waves are more persistent, so the droplet is more strongly influenced by its history[20].

For the range of parameters considered, $\gamma_F = 4.022g$. We focus on the statistical behaviour of a walker in the high-memory regime, specifically $\gamma/\gamma_F = 0.998$, thereby ensuring that, as in the original corral experiment[5], the characteristic decay time of the subharmonic Faraday waves, or 'memory' time $T_M = T_d/(1 - \gamma/\gamma_F) \sim 7.8$ s, exceeds the droplet's characteristic crossing time $T_c = a/u \sim 1.6$ s. Here, $T_d = \lambda_F^2/(8\pi^2\nu)$ is the wave decay time in the absence of vibrational forcing[21], λ_F is the Faraday wavelength as prescribed by the standard water-wave dispersion relation, and $u \sim 6–9$ mm s^{-1} is the characteristic speed of the droplet. If $T_M < T_c$, the waves decay faster than the droplet crosses the cavity and dissipation precludes the persistent wave field necessary for the emergence of the quantum-like statistical behaviour. The droplet motion was recorded for 3.5 h in 30 min intervals to maintain the prescribed memory, which may drift slowly owing to variations in viscosity and surface tension resulting from ambient temperature changes. γ_F was measured before and after each acquisition period and only data sets for which $|\Delta\gamma_F|/\gamma_F < 0.001$ were retained, where $\Delta\gamma_F$ represents the variation in the Faraday threshold over a 30 min segment. The Faraday threshold is never crossed: the bath surface would remain flat in the absence of the droplet.
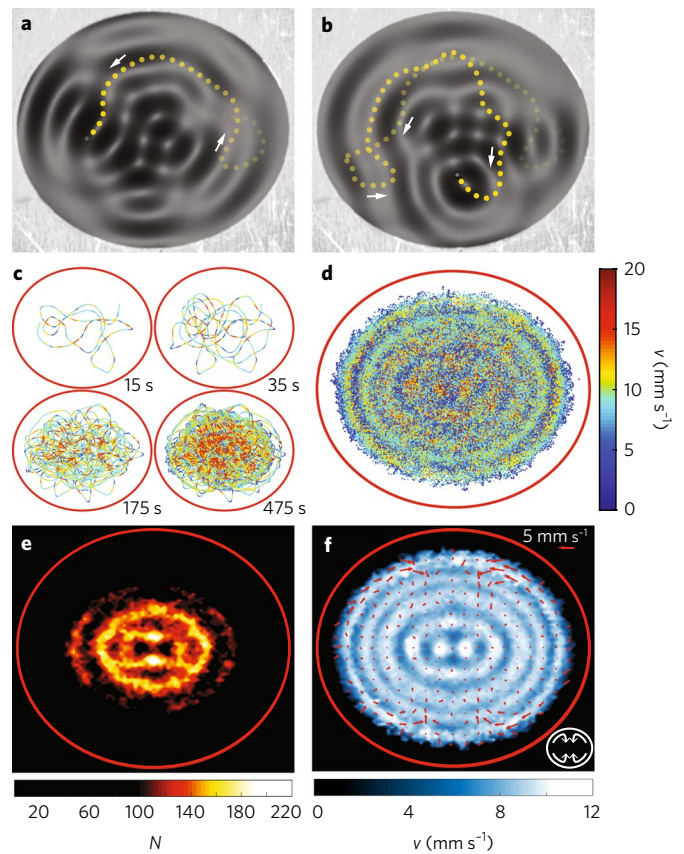

Fig. 2 | Droplet statistics in an elliptical corral. a,b, Top views illustrating the complex instantaneous wave field excited by the drop's motion along the yellow dashed trajectory (Supplementary Movie 1). **c,** Chaotic droplet trajectory, coloured according to the instantaneous speed, for increasing time intervals. **d,** Emergent pattern after 3.5 h. **e,** Histogram of the walker's position (90 × 90 bins). **f,** Local average speed (contour plot) and velocity (arrows) for the data shown in **d**. The absolute average speed is $\langle u \rangle = 8.68$ mm s^{-1}. Here, $f = 72$ Hz, $\gamma/\gamma_F = 0.998$ and $d = 0.79 \pm 0.01$ mm, for which the most unstable Faraday wave mode is the (1,5) mode illustrated in Fig. 3c,d.

In this high-memory regime, the droplet motion is highly irregular. Its trajectory is characterized by frequent and abrupt changes in direction and speed prompted by impacts on its complex pilot wave field. Figure 2a,b illustrate the spatio-temporal complexity of the instantaneous wave field and the associated droplet trajectory. See Supplementary Movie 1 for a longer time series. Note that the instantaneous wave field inside the corral is markedly different from both the distinct horseshoe shape arising for a free walker[20] and from the corral's most unstable Faraday mode, whose form is evident in Fig. 3c. Figure 2c shows the drop trajectory, colour-coded according to speed, for paths of increasing length. Eventually, a well-defined pattern emerges, revealing a correlation between drop position and speed (Fig. 2d). The histogram of the walker position (Fig. 2e) reveals sharply defined regions that the walker visits more frequently, including two small circular regions near the centre of the ellipse and enclosing elliptical rings whose intensity decreases outwards. The average speed map presented in Fig. 2f shows that peaks in the histogram correspond to regions of lower speed, as is also indicated in Fig. 2d. Figure 2f shows an overlay of the average velocity (arrows), which is effectively zero in the centre of the corral, indicating that the droplet visits each point there with some characteristic speed but with a random direction. Conversely, near the borders of the corral, an apparent quadrupole stream emerges in the mean velocity field. Specifically, the walker has a tendency to move along
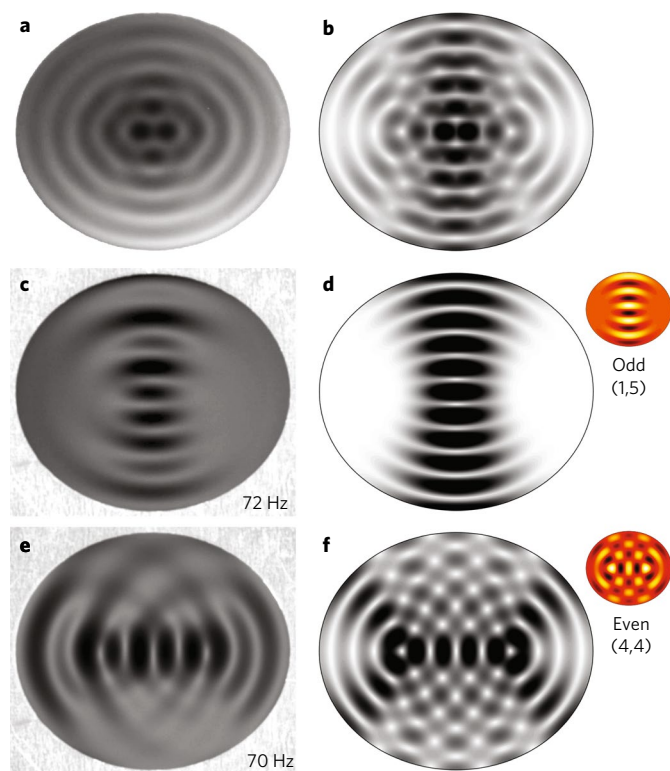
Fig. 3 | Mean pilot-wave field. a, Mean pilot-wave field obtained by averaging the instantaneous waves, such as those shown in Fig. 2a,b, over 30 min. Note that at the prescribed acceleration ($\gamma < \gamma_F$), no waves would exist in the absence of the drop. **b**, Superposition of the analytical gradient maps presented in **d** and **f**, showing good agreement with the mean wave pattern (**a**) and so the walker's statistical response (Fig. 2e,f). **c,e**, Faraday waves observed at threshold $\gamma = \gamma_F$ with $f = 72$ Hz (**c**) and 70 Hz (**e**). **d,f**, The patterns in **c** and **e** are well approximated by the two analytical eigenfunctions in **d** and **f**, respectively, which correspond to solutions of the Helmholtz equation in an elliptical domain with Dirichlet boundary conditions. In **d** and **f**, right, the eigenmodes are depicted in bright colours, while the greyscale figures show the magnitude of their spatial gradients, with white corresponding to zeros in slope (extrema or saddle points) and black corresponding to extrema in slope. This depiction allows for a direct comparison between the analytical modes and experimental visualization of the waves[17].

Fig. 4 | Fundamental modes of the elliptical corral transiently excited by the walker. On rare occasions when the walker's trajectory coincides with one of the crests or troughs of the fundamental Faraday modes for an extended period, a pilot-wave form resembling the corral's fundamental Faraday modes may briefly appear. **a,b**, The (4,4) Faraday mode dominant at 70 Hz emerges in the bath. **c,d**, The (1,5) Faraday mode dominant at 72 Hz becomes apparent. The yellow dotted line illustrates the droplet's trajectory. Here, $\gamma/\gamma_F = 0.998$ and $f = 72$ Hz.

the border from the ends of the major axis towards the ends of the minor axis, where it then recirculates towards the corral centre.

Averaging the highly irregular instantaneous wave field (Fig. 2a,b) over 30 min reveals a well-defined mean wave field (Fig. 3a) with features strikingly similar to those characterizing the position histogram and average speed map (Fig. 2e,f). The brighter areas in the mean wave field represent regions whose average slope is zero and coincide with high-density and low-speed regions in the position histogram and speed map, respectively. This correspondence indicates that the walker's statistical response is slaved to the mean wave field through the relatively incoherent, particle-centred, instantaneous pilot wave.

To rationalize this correspondence, we turn our attention to the Faraday waves emerging inside the corral, in the vicinity of the driving frequency, just above the Faraday threshold. It is important to distinguish these standing Faraday wave modes, which appear above threshold in the absence of the walker, from the instantaneous wave fields (for example Fig. 2a,b) excited at $\gamma < \gamma_F$ by the walking drop, which decay both in time and space. Figure 3c,e shows the Faraday waves observed at threshold $\gamma = \gamma_F$ with $f = 72$ and 70 Hz, respectively, which are well approximated by particular solutions of the Helmholtz equation for an elliptical membrane with
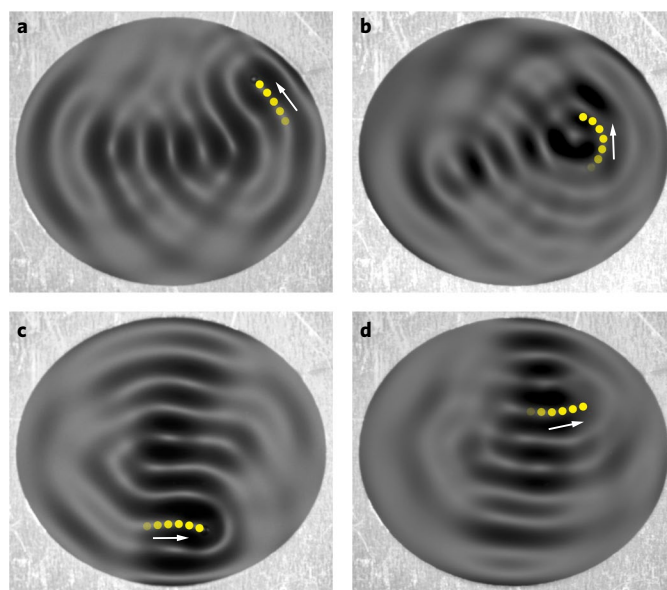
Dirichlet boundary conditions. Specifically, the waves observed at $f = 72$ Hz (Fig. 3c) correspond to the odd (1,5) elliptical eigenfunction (Fig. 3d), while those found at $f = 70$ Hz correspond to the even (4,4) mode[22]. We note that Dirichlet boundary conditions are the most appropriate given the minimal thickness of the fluid film surrounding the cavity and the resulting tendency of surface tension and viscosity to minimize the wave amplitude there[23].

By superposing the (1,5) and (4,4) wave modes in equal weight as a first approximation, we find the pattern presented in Fig. 3b, whose main features correspond closely to those of the mean wave field shown in Fig. 3a and consequently to the walker's position histogram and speed map in Fig. 2e,f. This correspondence indicates that the walker's seemingly chaotic motion is actually being dictated by the resonant Faraday modes of the cavity, some combination of which is subcritically ($\gamma < \gamma_F$) excited at each impact. In this particular case, the walker appears to be exciting not only the Faraday mode at the driving frequency ($f = 72$ Hz) but also a second mode that is dominant at a nearby frequency ($f = 70$ Hz). The presence of other modes with relatively small weights cannot be discounted. We note that each drop impact must excite other eigenmodes in order to give rise to the intricate instantaneous wave field observed experimentally (Fig. 2a,b). It is only in some exceptional occasions, when the walker happens to move along one of the main crests or troughs of one of the two fundamental cavity modes for an extended period, that the instantaneous wave resembles either of these two modes (Fig. 4). At each impact, the walker is thus exciting some collection of modes, two of which (the (1,5) and (4,4) modes) are predominant, their relative weight depending on the drop position and recent trajectory. The remaining rapidly decaying modes evidently have no significant effect on the mean wave field or the droplet statistics. The mean wave field also indicates that, on average, the dominant modes are being excited equally. We note that it has been shown that averaging chaotic Faraday waves well above threshold ($\gamma \gg \gamma_F$), in the absence of a walker, also yields a mean field related to the linear wave modes of the cavity[24].

We now focus on demonstrating how localized topographic features in the form of submerged circular wells can vary the mode balance by diminishing or enhancing the resonance of specific cavity eigenmodes and so alter drastically the statistical response of the walking droplet. We machined a cylindrical well of diameter $D = 5.5$ mm and depth $H = 4.5$ mm on the bottom of the elliptical corral (Fig. 1c) and repeated the experiment under precisely the same conditions as those in Fig. 2. Because γ_F decreases for increasing liquid depth, the well is essentially generating a spatially varying memory distribution, and the effective local memory above the well is larger than elsewhere. Although we ensure that $\gamma < \gamma_F$ everywhere, drop-induced surface disturbances are larger in amplitude and more persistent above the well due to the local diminution of the rate of viscous dissipation. The submerged well can thus be thought of as playing the role of the impurity in the quantum corral: by encouraging the emergence of localized high-amplitude perturbations in the underlying wave field through topologically induced changes in the local memory γ/γ_F, it enhances the resonance of specific cavity modes.

Two distinct configuration are considered: (1) the well is located at the midpoint of the upper semi-minor axis; (2) the well is placed at the left focus (Fig. 1d,e). The position histogram for the first configuration is presented in Fig. 5a. In this case, we find that the impurity substantially diminishes the resonance of the dominant fundamental modes. By comparing Fig. 5a with Fig. 2e, we observe a drastic decrease in the definition of the histogram: only weak traces of the fundamental modes are visible, along with localized high-density regions near the well. The latter indicate that the submerged well acts to attract the walker. The presence of the well also has noticeable effects in the walker's kinetics (Fig. 5c). Specifically, the speed map depicts a brighter area at the well's position, indicating that the droplet speed is higher in the deeper region, as is consistent with drop speed increasing with memory[20,21]. The average velocity map also underscores the attractive nature of the well. The direction of the arrows has changed in the upper half of the corral relative to the homogeneous corral (Fig. 5c), indicating that the walker now has a heightened tendency to move from the centre of the corral towards the well, along the upper semi-minor axis, then recirculate back towards the extremities of the major axis along the border of the corral. The mean wave field, now with reinforced horizontal bands in the centre, is presented in Fig. 5e. These features can be understood by examining the associated Faraday wave mode (Fig. 5g), which cannot be represented by a single eigenfunction. Placing the well at the midpoint of the semi-minor axis evidently induces more than one cavity mode. We note that placing the well in a relatively low-symmetry position, for example on a diagonal, has a similar effect: a relatively incoherent mixture of cavity modes is induced.

A markedly different response is observed when the well is located at a focus of the elliptical corral. In this case, the well enhances the resonance of a particular mode with maxima near the foci. Specifically, the presence of the well results in the (4,4) mode, found at 70 Hz in the homogeneous corral, becoming resonant at 72 Hz (Fig. 5h). This topologically induced effect has a drastic impact on the statistical behaviour of the droplet, which becomes slaved to the new dominant (4,4) wave mode. As a consequence, the histogram of the droplet presented in Fig. 5b shows a markedly stronger signal, in which high-density vertical bands appear to be projected from focus to focus. The height of the histogram peaks above the foci is the same for the homogeneous corral (Fig. 2e), but adding the submerged well at one focus (Fig. 5b) causes the overlying peak to be roughly twice that of its counterpart over the empty focus. The intensified resonance of the (4,4) mode is also evident in the mean velocity field (Fig. 5d), where new preferred paths emerge, including a motion along the boundary from the left to the right side of the corral. The mean wave field (Fig. 5f) also shows reinforced vertical bands, providing further evidence of the enhanced weight of the (4,4) mode.
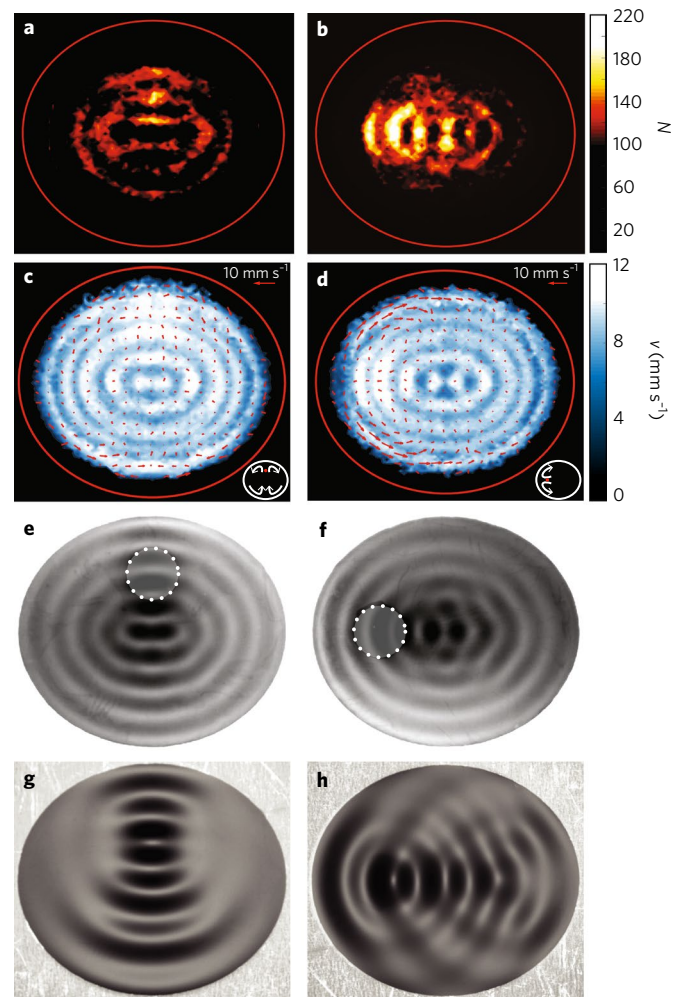

Fig. 5 | Resonant projection effects. a–f, Walker's histogram (**a,b**), average speed (colour map) and average velocity (arrows) (**c,d**) and mean wave field (**e,f**), arising when a submerged circular well is placed at the midpoint of the upper semi-minor axis (left column) or the left focus (right column). The well's diameter and depth are $D = 5.5$ mm and $H = 4.5$ mm, respectively, and its specific locations are indicated in **e** and **f**. The experimental parameters are as in Fig. 2. When the well is off focus (**a**), the resonance of the fundamental modes is notably obstructed: the histogram only shows traces of the statistical signature observed within a homogeneous corral (Fig. 2e). Conversely, when the well is at the focus (**b**), the resonance of the (4,4) mode is drastically enhanced, leading to a radical change in the walker's statistical behaviour, now characterized by high-density vertical bands projected towards the empty focus. This resonant effect is also evident in the corresponding average speed and average velocity maps (**c,d**), which show the emergence of substantially stronger mean velocities when the well is at the focus. In **e** and **f**, the mean pilot-wave field is shown averaged over 30 min, showing reinforced horizontal (**e**) and vertical (**f**) bands with respect to Fig. 3a due to the effects of the well. **g,h,** Faraday waves observed at threshold $\gamma = \gamma_F$ with $f = 72$ Hz when a submerged well is placed as in **e** and **f**. In both cases, the well induces waves markedly different from those observed at the same f with homogeneous topography (Fig. 3c). Specifically, the well at the focus enhances the (4,4) mode observed at 70 Hz in the absence of the well (Fig. 3e).

It is constructive to discuss the similarities with and differences between our experimental results and the controlled mode superposition and projection effects arising in elliptical quantum corrals[12,13]. The most striking difference is the vast disparity in scales between these macroscopic and microscopic systems. In the

quantum experiment, the characteristic corral size and electron speed are $a \sim 75\,\text{Å}$ and $u = h/(m\lambda_{dB}) \sim 2.5 \times 10^5\,\text{m s}^{-1}$, respectively[11], while the equivalent parameters are $a \sim 15\,\text{mm}$ and $u \sim 9\,\text{mm s}^{-1}$ in the walking droplet experiment. The walking droplet system is a driven dissipative classical system for which the spatial decay rate of the waves imposes an upper bound on the size of the cavity. Although 84 electrons were bounded within the quantum corral in the experiments of Manoharan et al.[13], the theoretical modelling of the quantum corrals is based on a single-particle description[11]. Our experiments demonstrate how a similar behaviour may emerge from a single-particle hydrodynamic pilot-wave system. Another similarity between the hydrodynamic and quantum corrals has been brought to light by our study. The statistics in a topologically homogeneous corral at 72 Hz are prescribed by the superposition of two fundamental cavity modes. One might thus surmise that this particular bouncing droplet experiment is essentially a mixed-state system characterized by a two-level Hamiltonian[25].

We have demonstrated striking new similarities between hydrodynamic and quantum corrals. We have shown that the statistical behaviour of the walker in a homogeneous elliptical corral can be described in terms of the superposition of a number of statistical states, a fundamental feature of quantum mechanics. Furthermore, we have demonstrated that a localized irregularity in the medium can drastically change the relative weight of the resonant modes and thus the statistical response of the confined droplet. As in the quantum corral experiments[12,13], we have shown that the position of the irregularity plays a critical role in the resulting statistical behaviour. High-symmetry configurations (specifically, with the well at the midpoint of the semi-minor axis) do not necessarily enhance the resonance of a particular cavity mode. However, when the impurity is placed at a focus, the walker induces a specific mode with maxima near the foci, leading to drastic changes in the statistical behaviour, including resonant projection towards the empty focus. Although these projection effects are directly evident in our hydrodynamic system, they only become apparent in quantum corrals by subtracting the standing waves that arise with and without the impurity[11]. The quantum mirage, a projection effect in the differential conductance, results directly from the sensitivity of the local conductivity to the altered statistical response. New challenges posed by our study include the determination of analogues in the walking droplet system of electric current and differential conductance in quantum corrals.

In the context of hydrodynamic quantum analogues[4], our study represents a significant advance. In previous studies, the fluid depth was sufficiently large that the pilot waves could be described in terms of deep-water waves. Here, we have demonstrated that hydrodynamic pilot-wave dynamics is viable in relatively shallow water, where the lower boundary influences the walking droplet's dynamics without entirely suppressing the Faraday waves[26]. Variations in topography may thus be used to generate spatial gradients in memory, effectively allowing for topographically induced potentials. Finally, we have characterized the mean pilot-wave field within the corral and demonstrated that its form is equivalent to the position histogram of the droplet and so also related to the fundamental modes of the cavity. While the focus of this study has been on effects akin to quantum superposition and projection, our results motivate consideration of hydrodynamic corrals of different geometries that will allow for quantitative comparative studies with quantum chaos in corrals[27] and quantum-mechanical pilot-wave theories[28].

Data availability

The data that support the findings of this study are available from the corresponding author upon reasonable request.

References

1. Couder, Y., Protière, S., Fort, E. & Boudaoud, A. Dynamical phenomena: walking and orbiting droplets. *Nature* **437**, 208–208 (2005).
2. Protière, S., Boudaoud, A. & Couder, Y. Particle–wave association on a fluid interface. *J. Fluid Mech.* **554**, 85–108 (2006).
3. Andersen, A. et al. Double-slit experiment with single wave-driven particles and its relation to quantum mechanics. *Phys. Rev. E* **92**, 013006 (2015).
4. Bush, J. W. M. Pilot-wave hydrodynamics. *Annu. Rev. Fluid Mech.* **47**, 269–292 (2015).
5. Harris, D. M., Moukhtar, J., Fort, E., Couder, Y. & Bush, J. W. M. Wavelike statistics from pilot-wave dynamics in a circular corral. *Phys. Rev. E* **88**, 011001 (2013).
6. Crommie, M. F., Lutz, C. P. & Eigler, D. M. Confinement of electrons to quantum corrals on a metal surface. *Science* **262**, 218–220 (1993).
7. Shirokoff, D. Bouncing droplets on a billiard table. *Chaos* **23**, 013115 (2013).
8. Gilet, T. Dynamics and statistics of wave-particle interactions in a confined geometry. *Phys. Rev. E* **90**, 052917 (2014).
9. Gilet, T. Quantumlike statistics of deterministic wave-particle interactions in a circular cavity. *Phys. Rev. E* **93**, 042202 (2016).
10. Kondo, J. Resistance minimum in dilute magnetic alloys. *Prog. Theor. Phys.* **32**, 37–49 (1964).
11. Fiete, G. A. & Heller, E. J. Theory of quantum corrals and quantum mirages. *Rev. Mod. Phys.* **75**, 933–948 (2002).
12. Moon, C. R., Lutz, C. P. & Manoharan, H. C. Single-atom gating of quantum-state superpositions. *Nat. Phys.* **4**, 454–458 (2008).
13. Manoharan, H. C., Lutz, C. P. & Eigler, D. M. Quantum mirages formed by coherent projection of electronic structure. *Nature* **403**, 512–515 (2000).
14. Harris, D. M. & Bush, J. W. M. Generating uniaxial vibration with an electrodynamic shaker and external air bearing. *J. Sound Vibration* **334**, 255–269 (2015).
15. Harris, D. M., Liu, T. & Bush, J. W. M. A low-cost, precise piezoelectric droplet-on-demand generator. *Exp. Fluids* **56**, 83 (2015).
16. Couder, Y., Fort, E., Gautier, C.-H. & Boudaoud, A. From bouncing to floating: noncoalescence of drops on a fluid bath. *Phys. Rev. Lett.* **94**, 177801 (2005).
17. Douady, S. Experimental study of the Faraday instability. *J. Fluid Mech.* **221**, 383–409 (1990).
18. Faraday, M. On a peculiar class of acoustical figures; and on certain forms assumed by groups of particles upon vibrating elastic surfaces. *Phil. Trans. R. Soc. Lond.* **121**, 299–340 (1831).
19. Miles, J. & Henderson, D. Parametrically forced surface waves. *Annu. Rev. Fluid Mech.* **22**, 143–165 (1990).
20. Eddi, A., Sultan, E., Moukhtar, J., Fort, E., Rossi, M. & Couder, Y. Information stored in Faraday waves: the origin of a path memory. *J. Fluid Mech.* **674**, 433–463 (2011).
21. Moláček, J. & Bush, J. W. M. Drops walking on a vibrating bath: towards a hydrodynamic pilot-wave theory. *J. Fluid Mech.* **727**, 612–647 (2013).
22. Gutierrez-Vega, J. C., Rodriguez-Dagnino, R. M., Meneses-Nava, M. A. & Chavez-Cerda, S. Mathieu functions, a visual approach. *Am. J. Phys.* **71**, 233–242 (2003).
23. Blanchette, F. Modeling the vertical motion of drops bouncing on a bounded fluid reservoir. *Phys. Fluids* **28**, 032104 (2016).
24. Gluckman, B. J., Arnold, C. B. & Gollub, J. P. Statistical studies of chaotic wave patterns. *Phys. Rev. E* **51**, 1128–1147 (1995).
25. C. Cohen-Tannoudji, B. Diu & F. Laloë. *Quantum Mechanics* (Wiley, 1977).
26. Kumar, K. Linear theory of Faraday instability in viscous liquids. *Proc. R. Soc. Lond. A* **452**, 1113–1126 (1996).
27. Heller, E. J. Bound-state eigenfunctions of classically chaotic Hamiltonian systems: scars of periodic orbits. *Phys. Rev. Lett.* **53**, 1515–1518 (1984).
28. Bush, J. W. M. The new wave of pilot-wave theory. *Phys. Today* **68**, 47–53 (2015).

Acknowledgements

Author contributions

P.J.S. and J.W.M.B. conceived and developed the project. P.J.S. and T.C.-P. performed the experiments and reduced the data. P.J.S. and J.W.M.B. wrote the paper.

Competing interests

The authors declare no competing financial interests.

Additional information